PHOTONIC SENSORS / Vol. 9, No. 2, 2019: 126–134

High Sensitive Refractive Index Sensor Based on Cladding Etched Photonic Crystal Fiber Mach-Zehnder Interferometer

Haifeng DU, Xiaoyan SUN, Youwang HU*, Xinran DONG, and Jianhang ZHOU

State Key Laboratory of High Performance Complex Manufacturing, College of Mechanical and Electrical Engineering, Central South University, Changsha 410083, China

*Corresponding author: Youwang HU E-mail: huyw@csu.edu.cn

Abstract: A high sensitive refractive index sensor based on the cladding etched photonic crystal fiber (PCF) Mach-Zehnder interferometer (MZI) is proposed, which is spliced a section of photonic crystal fiber between two single modes fibers (SMFs).The interference fringe of the MZI shifts with the variation of the ambient refractive index (RI). It is found that the RI sensitivity slightly decrease with an increase in the interference length. The sensitivities of MZI with 35 mm PCF, 40 mm PCF, and 45 mm PCF are 106.19 nm/RIU, 93.33 nm/RIU, and 73.64 nm/RIU, respectively, in the range of 1.333 to 1.381. After etched, the RI sensitivity of the MZI could be improved obviously. The RI sensitivities of the MZI with 35 mm PCF are up to 211.53 nm/RIU and 359.37 nm/RIU when the cladding diameter decreases to 112 μm and 91 μm, respectively. Moreover, the sensor is insensitive to temperature, and the measured sensitivity is only 9.21 pm/℃ with the range from 20 ℃ to 500 ℃. In addition, the sensor has advantage of simple fabrication, low cost, and high RI sensitivity.

Keywords: Refractive index sensor; Mach-Zehnder interferometer; photonic crystal fiber; hydrofluoric acid

Citation: Haifeng DU, Xiaoyan SUN, Youwang HU, Xinran DONG, and Jianhang ZHOU, "High Sensitive Refractive Index Sensor Based on Cladding Etched Photonic Crystal Fiber Mach-Zehnder Interferometer," *Photonic Sensors*, 2019, 9(2): 126–134.

1. Introduction

Refractive index sensors can be used to measure the concentrations of gases and liquids, and are widely used in the biological and chemical environmental detection [1, 2]. There are two optical methods, the optical path measurement method and optical fiber measurement method, which are used to measure the refractive indices of liquids [3]. The optical path structure is complex, and the optical path is not stable. Optical fiber is widely used in the liquid refractive index test because of its light weight, small volume, strong electromagnetic interference resistance, and simple design [4]. Up to now, a number of optical fiber microstructures have been proposed for refractive index sensors, including long period fiber grating (LPFG) [5, 6], fiber Bragg grating (FBG) [7], Fabry-Perot interferometer (FPI) [8], and Mach-Zehnder interferometer (MZI) [9, 10]. These structures have high sensitivity in refractive index sensing. However, a serious disadvantage for the above structures is high sensitivity to the environmental temperature [11, 12]. Unlike traditional polarization maintaining photonic crystal fibers (PM-PCF), which contain at least two different glasses each with a different thermal expansion coefficient, the photonic crystal fiber birefringence is highly insensitive to the

Received: 27 July 2018 / Revised: 29 November 2018

DOI: 10.1007/s13320-019-0532-2
Article type: Regular

temperature [4, 13]. The optical fiber sensor based on the MZI with the PCF structure has the advantages of ease to fabricate and convenience to measure, which is a common method in the research of refractive index sensors.

In recent years, many novel in-line MZIs with the PCF structure have been proposed and studied. Y. Zhao *et al.* [14] proposed a PCF interferometer structure with up-tapered joints for RI sensing, which achieved a high RI sensitivity of 252 nm/RIU in the RI range of 1.333 – 1.379. D. Wu *et al.* [15] proposed an RI sensor based on a tapered PCF MZI structure with an RI sensitivity of 51.902 nm/RIU in the range 1.3411 – 1.3737. Y. Zhao *et al.* [16] reported a novel refractive index (RI) sensor based on the PCF-MZI which is fabricated by cascading a section of PCF with half-taper collapse regions (HTCRs) between two single mode fibers (SMFs) and investigated the RI sensitivity of 181.96 nm/RIU when the RI varied from 1.3333 to 1.3574. Dnyandeo Pawar *et al.* [17] proposed a tapered polarization maintaining photonic crystal fiber (PM-PCF) MZI sensor, and it had a sensitivity of 20.53 nm/RIU within the RI range from 1.33 to 1.37. These special structures of the MZI including tapered and cascading structure are complex to fabricate, time-consuming, and with low sensitivity. In order to improve the sensitivity of optical fiber sensors, many novel methods are proposed, such as chemical etching and coating on the optical fiber surface. Y. C. Tan *et al.* [18] presented a carbon nanotubes (CNT) deposited PCF featuring a Mach-Zehnder interferometer configuration for refractive index (RI) sensing. L. Melo *et al.* [19] reported an in-line MZI coated with hafnium oxide by atomic layer deposition to increase the RI sensitivity which was 1307 nm/SRI within the range of 1.3327 – 1.3634. However, the deposition techniques used usually involve highly precise equipment or a long fabrication duration due to the extensive amounts of chemical processes involved.

In this paper, we present a PCF MZI refractive index sensor, which is realized by splicing a piece of PCF between two standard single mode fibers with a fusion splicer. The result shows that the effective RI of high order modes of the PCF cladding is more sensitive and more linear to surrounding refractive index changing, so we select high order mode spectra as the experimental measurement data. With an increase in the PCF length (30 mm, 35 mm, and 40 mm), the RI sensitivity decreases gradually (106.19 nm/RIU, 93.33 nm/RIU, and 73.64 nm/RIU) within the RI range of 1.333 – 1.381. Afterwards, we adopt a novel method of etching the surface of photonic crystal fiber (the PCF length of 35 mm) by using hydrofluoric acid (HF) to enhance the RI sensitivity. The refractive index sensitivity increases to 359.37 nm/RIU when the cladding diameter decreases to 91 μm. With a decrease in the cladding diameter, the sensitivity of refractive index will be improved obviously. In addition, the PCF-MZI has advantages of temperature insensitivity, simple fabrication, low cost, and high RI sensitivity.

2. Sensor fabrication and principle

2.1 Design of MZI

The schematic of the sensor structure is shown in Fig. 1. The sensor is composed of SMFs and one segment of PCF (NKT Photonics LMA-10). The PCF is sandwiched to SMFs (Corning SMF-28). They are spliced together directly by a commercial fusion splicer (Fujikura 80S), and the splicing loss is about 1 dB. Figure 1(b) shows the scanning electron micrograph (SEM) of the cross section of the PCF. The PCF has an outside diameter of 125 μm, a core diameter of 10 μm, a hole diameter of 2.85 μm, and a hole pitch of 7 μm. The standard single mode fiber has an outside diameter of 125 μm and a core diameter of 9 μm. Figures 1(a) and 1(c) show the schematic diagram and optical micrograph of the MZI with the PCF structure. Through many experimental results, we find that a high fringe

contrast suitable for fusion parameters can be obtained by tuning the arc power and arc time are +60 bit (the discharge intensity of standard is 0) and 380 ms, and the overlap value is 20 μm, respectively. From the collapsed region in Fig. 1(c), we can know that the air holes of the PCF have slight collapse. However, the collapse of air holes will increase the mode field diameter and make the energy between the two modes of interference more balanced, which is more conducive to the formation of interference and increase the contrast of spectral fringes [20, 21]. A light source and an optical spectrum analyzer are connected to monitor the spectrum change during the fabrication.

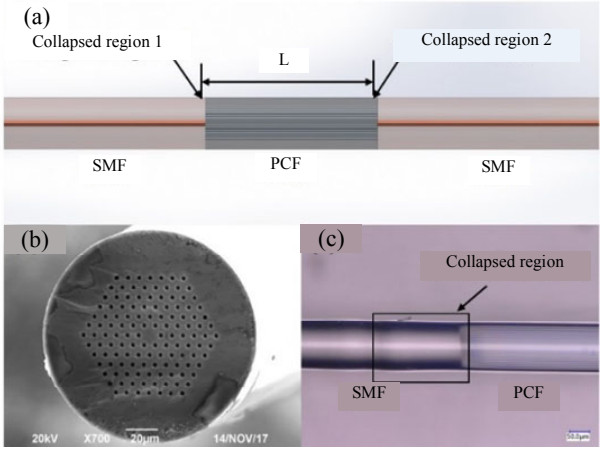

Fig. 1 In-line MZI with the PCF structure (a) schematic diagram of the MZI, (b) scanning electron micrograph (SEM) of the cross section of a LMA-10-PCF, and (c) optical micrograph of the MZI.

2.2 Principle of the MZI

Figure 1 shows the in-line MZI with the PCF structure. A piece of PCF is spliced between two standard single mode fibers directly. When light travels from the SMF to the PCF, the fundamental mode of the SMF begins to diffract. In the first collapsed region, both the core and cladding modes with different propagation constants are excited. The interference spectrum can be expressed using the following two-beam optical interference equation [14, 22]:

$$I = I_1 + I_2 + \sqrt{I_1 I_2}\cos\beta \tag{1}$$

where I is the intensity of the total interference signal, and I_1 and I_2 are the intensities of the core and cladding modes, respectively. The phase difference β between the core and clad modes of an MZI is expressed as

$$\beta = \frac{2\pi\Delta n_{\text{eff}} L}{\lambda} \tag{2}$$

where L is the interference length, λ is the wavelength of propagating light, and Δn_{eff} is the difference between the effective refractive indices of core and cladding modes, $\Delta n_{\text{eff}} = n_{\text{eff}}^{\text{core}} - n_{\text{eff}}^{\text{clad}}$. When the difference between the cladding mode and core mode equals to $(2m+1)\pi$, the m-order interference valley is shown as follows:

$$\lambda_m = \frac{2\Delta n_{\text{eff}} L}{2m+1}. \tag{3}$$

The free spectrum range (FSR) of the interference spectrum can be defined as follows:

$$\Lambda = \frac{\lambda^2}{\Delta n_{\text{eff}} L}. \tag{4}$$

The wavelength of the m-order interference valley varies along with the surrounding refractive index, and the variation is shown as

$$\Delta\lambda_m = \frac{2(\Delta n_{\text{eff}} + \Delta n)L}{2m+1} - \frac{2\Delta n_{\text{eff}} L}{2m+1} = \frac{2\Delta n L}{2m+1} \tag{5}$$

where Δn is the variation of the effective refractive index of the photonic crystal fiber cladding along with surrounding refractive index changing.

2.3 Experimental measurement method

The schematic diagram of our experimental measurement is shown in Fig. 2. A broadband light source (C+L, Shanghai Hanyu) with a wavelength range of 1528 nm – 1602 nm is launched into the MZI structure. There is an optical path difference when light transmits through the sensor, and the interference will happen at the second collapsed region. The interference spectrum can be monitored by using an optical spectrum analyzer (OSA, Agilent 86142B, 600 nm – 1700 nm). The sensor is attached to the bottom of the glassware during testing the RI changes.

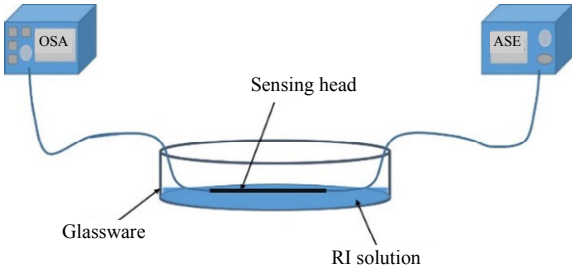

Fig. 2 Schematic diagram of the experimental measurement.

3. Results and discussion

Different parameters influence the properties and performances of the PCF interferometer, such as arc time, arc power, interference length, and the diameter of the PCF. These factors should be considered during the fabrication of the PCF interferometer. In this paper, the effects of the interference length on the interference spectrum and the sensitivity of RI sensing are investigated experimentally. Three kinds of PCF interferometer with different interference lengths of 30 mm, 35 mm, and 40 mm are made by using the same welding parameters. The transmission spectra of a PCF interferometer with different sensing lengths in air and water are shown in Fig. 3. From Fig. 3, we can see some interference peaks with the low fringe contrast when the sensor is immersed in air, which are caused by multimode interference. When the sensor is immersed in water, the wavelength is red-shift, and the interference peaks caused by multimode interference are decreased because the refractive index of water is higher than that of air, and the multimode interference is suppressed in water. The interference peaks produced by multi-mode interference have a small influence on sensing.

In air, λ_m (the wavelength of the m-order interference valley) is 1585.74 nm, 1575.68 nm, and 1583.81 nm, and the fringe spaces ranges (Λ) for the three PCF interferometers with the interference length of 30 mm, 35 mm, and 40 mm are 25.5 nm, 18.9 nm, and 16.2 nm, respectively. This result shows that the average fringe period decreases with an increase in the interferometer length, which is in conformity with the theory of interference in (4). According to (3) and (4), we can calculate the Δn_{eff} = 0.0033, 0.0038, and 0.0039, and m=62, 84, and 98 for the PCF lengths of 30 mm, 35 mm, and 40 mm, respectively. According to (5), we know that the refractive index sensitivity is proportional to the PCF length (L) and inversely proportional to interference mode (m).

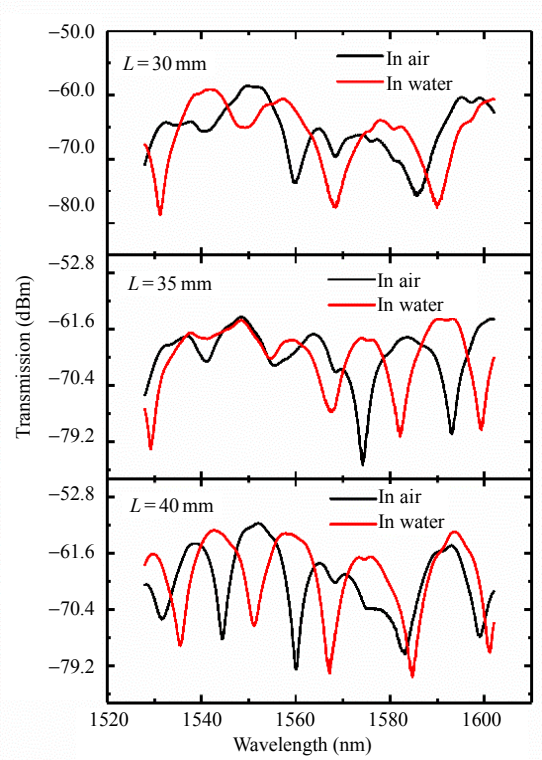

Fig. 3 Transmission spectra of a PCF interferometer with different sensing lengths in air and water.

The ability of the PCF interferometer to detect the change of RI in the liquid environment is studied. The refractive index solution is formed by mixing water with glycerol in a certain proportion, and it ranges from 1.333 to 1.381 in the experiments. Figures 4(a), 4(b), and 4(c) are the spectral change diagrams of three different lengths PCF interferometers in different refractive index liquids. With an increase in the refractive index, the wavelength of the interference spectrum appears red-shift. The relationship between the maximum wavelength shift amount and refractive index of three different lengths PCF interferometers are

illustrated in Fig. 4(d) by linear fitting. The maximum refractive index sensitivities of the PCF interferometer with the interference length of 30 mm, 35 mm, and 40 mm are around 106.19 nm/RIU, 93.33 nm/RIU, and 73.643 nm/RIU, respectively, and the corresponding fitting degrees (R^2) are 0.99234, 0.99643, and 0.98433, respectively. The results show that the refractive index sensitivity of the PCF interferometer decreases with an increase in the interference length.

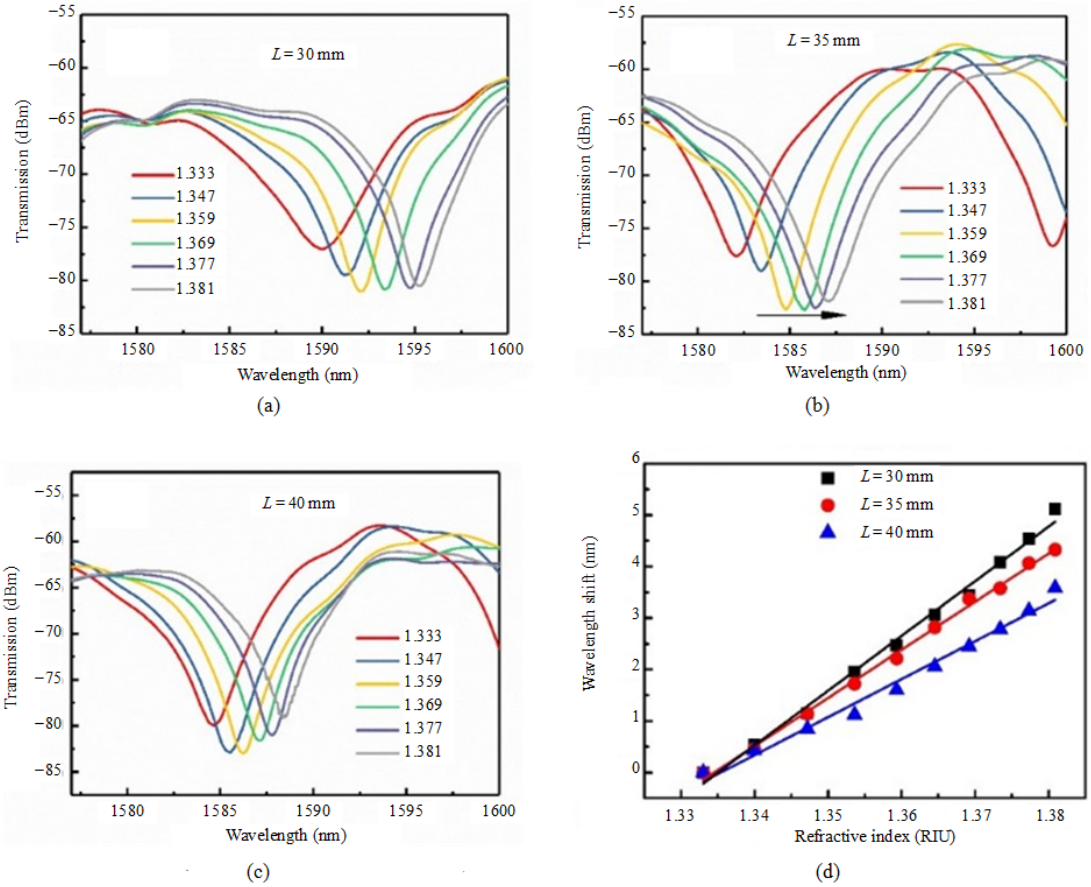

Fig. 4 Spectral change diagram of three different lengths PCF interferometers in different refractive index liquids (a) L=30 mm, (b) L=35 mm, (c) L=40 mm, and (d) relationship between the wavelength shift and surrounding RI of the PCF interferometer with different etching time.

In order to improve the refractive index sensitivity of the PCF interferometer, in this experiment, an HF etching method is used to corrode the PCF with a length of 35 mm because it has a better corresponding fitting degree, and the concentration of HF is 20%. Figure 5 shows the different diameters of the PCF under the microscope, and the diameter is 125 μm (no etching), 112 μm (etching for 10 min), and 91 μm (etching for 80 min), respectively. Figure 6 shows the transmission spectra of the MZI with different etching time in air. With an increase in the etching time, the wavelength of the interference spectrum appears blue-shift, and the transmission loss decreases gradually. Figures 7(a), (b), and 7(c) show the spectral change diagrams of the 35 mm MZI with different etching time when liquid RI varies. A red shift in the spectrum is observed when RI increases from 1.333 to 1.381, and total wavelength shift amounts of the PCF interferometer before corrosion, and the etching

time for 10 min and 80 min are 4.326 nm, 9.867 nm, and 16.643 nm, respectively. The RI sensitivities are obtained to be 93.33 nm/RIU, 211.53 nm/RIU, and 359.37 nm/RIU by linear fitting, and they have better corresponding fitting degrees (0.99643, 0.99553, and 0.99661, respectively), as shown in Fig. 7(d). Considering the wavelength resolution (10 pm) used by the OSA in this experiment, the resolution of RI index limit is 1.07 $\times 10^{-4}$ RIU, 4.73 $\times$ 10^{-5} RIU, 2.78 $\times$ 10^{-5} RIU, respectively, within the range from 1.333 to 1.381.

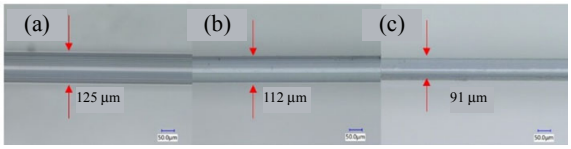

Fig. 5 Different diameter of PCF under the microscope.

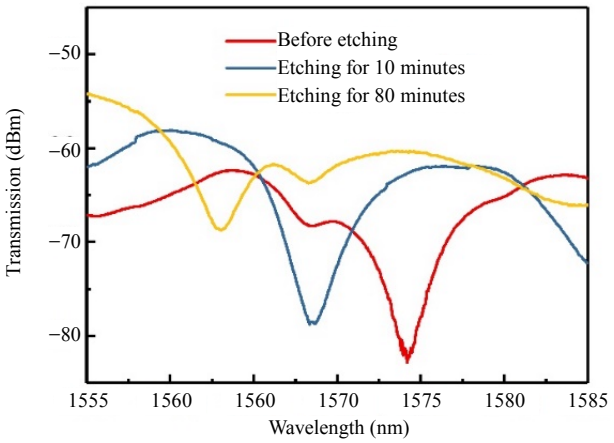

Fig. 6 Transmission spectra of PCF interferometer with different etching time in air.

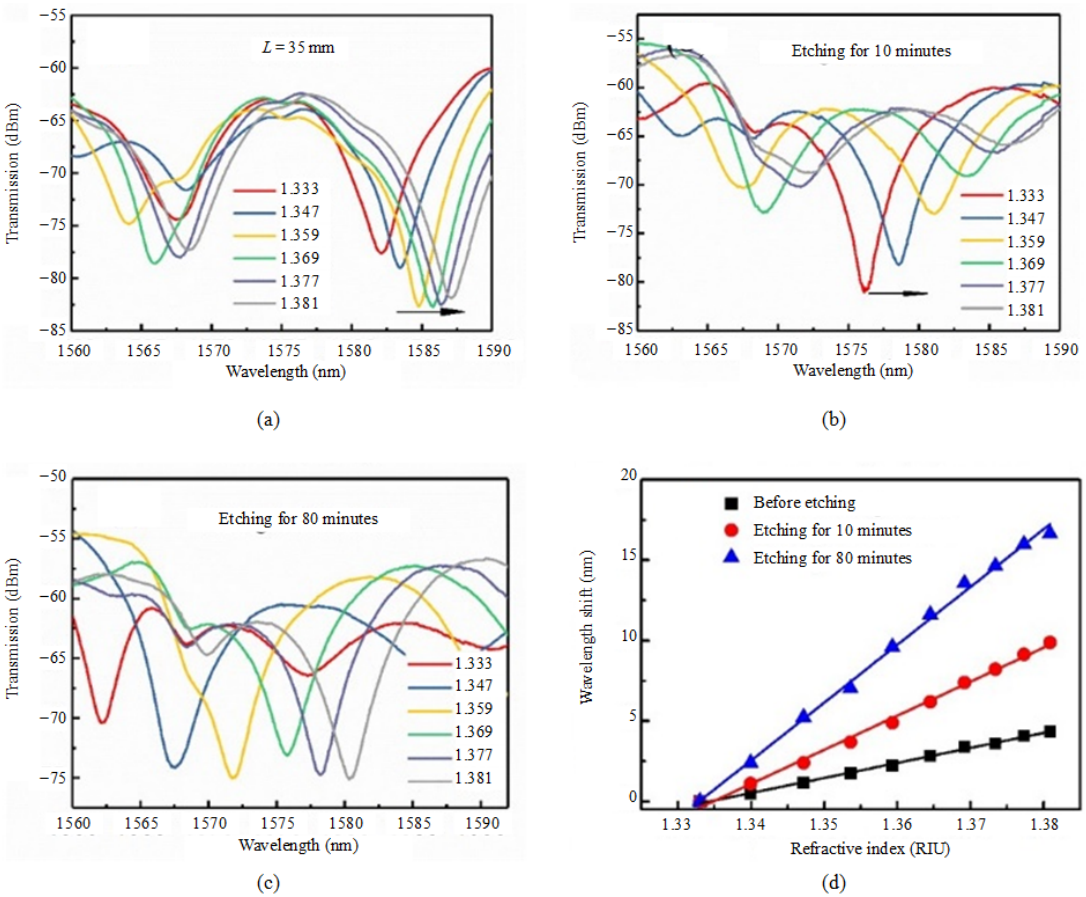

Fig. 7 Spectral change diagrams of (a) before corrosion, (b) etching for 10 minutes, (c) etching for 80 minutes, and (d) relationship between wavelength shift and surrounding RI of PCF interferometer with different etching time.

It can be seen that the RI sensitivities of the PCF interferometer are improved evidently with an increase in the etching time. The reason is that the PCF diameter is decreased by the HF etching method. When the surrounding RI is a constant, a PCF diameter decrease will result in an increase in Δn_{eff} as expressed in (5). That is to say, the interaction between the evanescent waves of the cladding modes and the ambient environment around the fiber will be enhanced, so the influence of the surrounding refractive index changing on the transmission characteristics of the cladding mode is more obvious.

Because the PCF has a micro-hole structure which has a small coefficient of thermal expansion, the main advantage of the PCF is that it is insensitive to the temperature. In order to prove that temperature has less influence on the refractive index measurement, a 35 mm PCF interferometer is heated from 20 ℃ to 500 ℃. The transmission spectra of this PCF interferometer are shown in Fig. 8(a). The relationship between the wavelength shift and temperature is shown in Fig. 8(b), and the temperature sensitivity is 9.21 pm/℃. As the environmental temperature change is about 10 ℃, the corresponding wavelength shift of the PCF interferometer is less than 0.1 nm. Our experimental temperature is 20 ℃, and the range of temperature fluctuation is slight (within 2 ℃ fluctuation). This means that temperature has less influence on the refractive index measurement, which could be ignored compared with the RI sensitivity.

A comparison between the proposed MZI and related MZIs based on the splicing technology is listed in Table 1. Table 1 shows that the sensitivities of the proposed sensor have higher RI sensitivity than PCF with up-tapered joints (252 nm/RIU) [14], PCF-MZI with two HTCRS (181.96 nm/RIU) [16], and MMF (Multimode fiber)-SMF-MMF (–37.93 nm/RIU) [25]. Because the diameter of the corroded PCF decreases, the interaction between the evanescent wave of cladding mode and the surrounding environment of the fiber is enhanced. However, the sensor we reported has lower sensitivity than the open-cavity MZI (–1364.343 nm/RIU), but the open-cavity MZIs usually have small RI measurement range (only 1.333 – 1.3468) although they have ultrahigh RI sensitivity. Because the PCF is insensitive to the temperature, the temperature sensitivity of the proposed PCF interferometers (9.21 pm/℃) is almost the same with that of other PCF structure interferometers, but they are lower than that of the SMF structure MZIs, such as small offset with the SMF (49 pm/℃) [24] and open-cavity MZI [26].

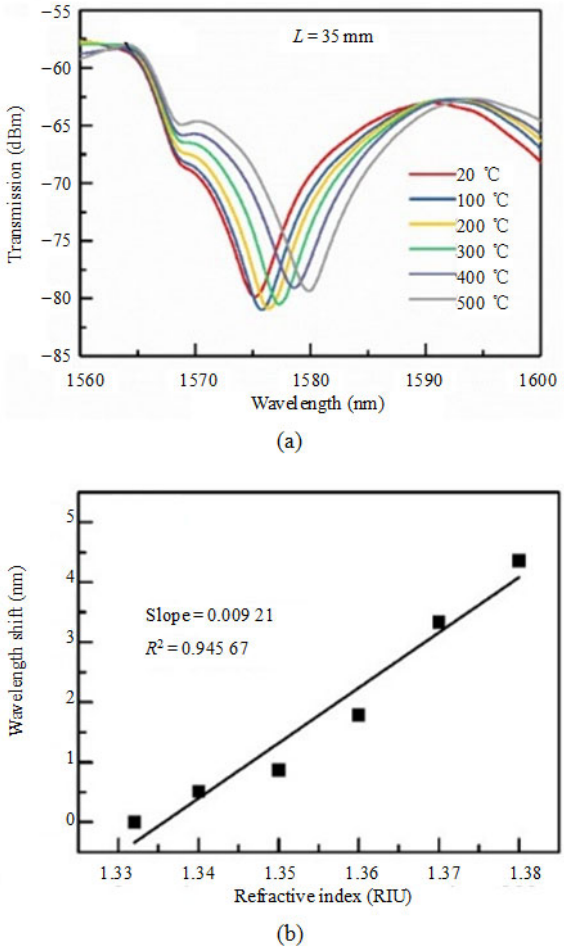

Fig. 8 Results of temperature response experiment: (a) transmission spectra of the PCF interferometer and (b) relationship between the wavelength shift and temperature.

Table 1 Comparison between the available MZI sensors and the proposed MZI.

Sensor structure	Refractive sensitivity (nm/RIU)	Refractive range	Temperature sensitivity (pm/℃)	Temperature range (℃)	Reference
PCF with up-tapered joints	252	1.333–1.379	2.96	20–170	[14]
PCF taper structure	51.902	1.3411–1.3737	0.9	20–50	[15]
PCF-MZI with two HTCRS	181.96	1.3333–1.3574	−	−	[16]
MZI based on step-like tapers	−185.79	1.3333–1.3673	−	−	[23]
Small offset with SMF	−38.1	1.333–1.3739	49	20–50	[24]
MMF-SMF-MMF	−37.93	1.3105–1.3571	52.2	25–85	[25]
open-cavity MZI	−1364.343	1.333–1.3468	33	20–100	[26]
This work	359.37	1.333–1.381	9.21	20–500	

4. Conclusions

The paper proposes and studies a high sensitive refractive index sensor based on the Mach-Zehnder interferometer sensor, which splices a section of photonic crystal fiber (PCF) between two SMFs. The RI sensitivity of the MZI with the 35 mm PCF is enhanced obviously by HF etching with different time. In the RI range of 1.333 to 1.381, the RI sensitivity is 93.33 nm/RIU non-corrosion, which is up to 211.53 nm/RIU and 359.37 nm/RIU after 10 min and 80 min HF corrosion, and the temperature sensitivity is 9.21 pm/℃ with the temperature range from 20℃ to 500℃. In addition, the PCF-MZI has advantages of temperature insensitivity, simple fabrication, low cost, and high sensitivity, which is widely used in the biological and chemical environmental detection.

Acknowledgement

This research work is supported by the National Natural Science Foundation of China (NSFC) (Grant Nos. 51475482, 51875584, 51875585, and 51475481), the National Key R&D Program of China (Grant Nos. 2017YFB1104800 and 2018YFB1107803), and the Fundamental Research Funds for the Central Universities of Central South University.

References

[1] X. Y. Sun, X. R. Dong, Y. W. Hu, H. T. Li, D. K. Chu, J. Y. Zhou, *et al.*, "A robust high refractive index sensitivity fiber Mach-Zehnder interferometer fabricated by femtosecond laser machining and chemical etching," *Sensors & Actuators A: Physical*, 2015, 230: 111–116.

[2] J. H. Wo, G. H. Wang, Y. Cui, Q. Sun, R. B. Liang, P. Shum, *et al.*, "Refractive index sensor using microfiber-based Mach-Zehnder interferometer," *Optics Letters*, 2012, 37(1): 67–69.

[3] Q. Wang, L. X. Kong, Y. L. Dang, F. Xia, Y. W. Zhang, Y. Zhao, *et al.*, "High sensitivity refractive index sensor based on splicing points tapered SMF-PCF-SMF structure Mach-Zehnder mode interferometer," *Sensors & Actuators B: Chemical*, 2016, 225: 213–220.

[4] J. N. Wang and J. L. Tang, "Photonic crystal fiber Mach-Zehnder interferometer for refractive index sensing," *Sensors*, 2012, 12(3): 2983–2995.

[5] B. Y. Li, L. Jiang, S. M. Wang, H. L. Tsai, and H. Xiao, "Femtosecond laser fabrication of long period fiber gratings and applications in refractive index sensing," *Optics & Laser Technology*, 2011, 43(8): 1420–1423.

[6] F. Zou, Y. Q. Liu, C. L. Deng, Y. H. Dong, S. Zhu, and T. Y. Wang, "Refractive index sensitivity of nano-film coated long-period fiber gratings," *Optics Express*, 2015, 23(2): 1114–1124.

[7] W. Liang, Y. Huang, Y. Xu, R. K. Lee, and A. Yariv, "Highly sensitive fiber Bragg grating refractive index sensors," *Applied Physics Letters*, 2005, 86(15): 151122-1–151122-3.

[8] T. Wei, Y. K. Han, Y. J. Li, H. L. Tsai, and H. Xiao, "Temperature-insensitive miniaturized fiber inline Fabry-Perot interferometer for highly sensitive refractive index measurement," *Optics Express*, 2008, 16(8): 5764–5769.

[9] X. Y. Sun, D. K. Chu, X. R. Dong, C. Zhou, H. T. Li, L. Zhi, *et al.*, "Highly sensitive refractive index fiber inline Mach-Zehnder interferometer fabricated by femtosecond laser micromachining and chemical etching," *Optics & Laser Technology*, 2016, 77: 11–15.

[10] P. Lu, L. Q. Men, K. Sooley, and Q. Chen, "Tapered fiber Mach-Zehnder interferometer for simultaneous measurement of refractive index and temperature," *Applied Physics Letters*, 2009, 94(13): 131110-1–131110-3.

[11] X. R. Dong, Z. Xie, Y. X. Song, K. Yin, D. K. Chu, and J. A. Duan, "High temperature-sensitivity sensor based on long period fiber grating inscribed with femtosecond laser transversal-scanning method," *Chinese Optics Letters*, 2017, 15(9): 090602-1–090602-5.

[12] X. R. Dong, Z. Xie, C. Zhou, K. Yin, Z. Luo, and J. A. Duan, "Temperature sensitivity enhancement of platinum-nanoparticle-coated long period fiber gratings fabricated by femtosecond laser," *Applied Optics*, 2017, 56(23): 6549–6553.

[13] T. A. Birks, J. C. Knight, and P. S. J. Russell, "Endlessly single-mode photonic crystal fiber," *Optics Letters*, 1997, 22(13): 961–963.

[14] Y. Zhao, X. G. Li, L. Cai, and Y. Yang, "Refractive index sensing based on photonic crystal fiber interferometer structure with up-tapered joints," *Sensors & Actuators B: Chemical*, 2015, 221: 406–410.

[15] D. Wu, Y. Zhao, and J. Li, "PCF taper-based Mach-Zehnder interferometer for refractive index sensing in a PDMS detection cell," *Sensors & Actuators B: Chemical*, 2015, 213: 1–4.

[16] Y. Zhao, F. Xia, H. F. Hu, and M. Q. Chen, "A novel photonic crystal fiber Mach-Zehnder interferometer for enhancing refractive index measurement sensitivity," *Optics Communications*, 2017, 402: 368–374.

[17] D. Pawar and S. N. Kale, "Birefringence manipulation in tapered polarization-maintaining photonic crystal fiber Mach-Zehnder interferometer for refractive index sensing," *Sensors & Actuators A: Physical*, 2016, 252: 180–184.

[18] Y. C. Tan, Z. Q. Tou, V. Mamidala, K. K. Chow, and C. C. Chan, "Continuous refractive index sensing based on carbon-nanotube-deposited photonic crystal fibers," *Sensors & Actuators B: Chemical*, 2014, 202: 1097–1102.

[19] L. Melo, G. Burton, P. Kubik, and P. Wild, "Refractive index sensor based on inline Mach-Zehnder interferometer coated with hafnium oxide by atomic layer deposition," *Sensors and Actuators B: Chemical*, 2016, 236: 537–545.

[20] T. Zhu, F. F. Xiao, L. C. Xu, M. Liu, M. Deng, and K. S. Chiang, "Pressure-assisted low-loss fusion splicing between photonic crystal fiber and single-mode fiber," *Optics Express*, 2012, 20(22): 24465–24471.

[21] D. K. Sharma and A. Sharma. "Mode field expansion in index-guiding microstructured optical fibers," *SPIE*, 2013, 8794: 87942A-1–87942A-6.

[22] L. C. Li, L. Xia, Z. H. Xie, and D. M. Liu, "All-fiber Mach-Zehnder interferometers for sensing applications," *Optics Express*, 2012, 20(10): 11109–11120.

[23] Y. Zhao, M. Q. Chen, F. Xia, and H. F. Hu, "Spectrum online-tunable Mach-Zehnder interferometer based on step-like tapers and its refractive index sensing characteristics," *Optics Communications*, 2017, 403: 143–149.

[24] L. Cai, Y. Zhao, and X. G. Li, "A fiber ring cavity laser sensor for refractive index and temperature measurement with core-offset modal interferometer as tunable filter," *Sensors & Actuators B: Chemical*, 2017, 242: 673–678.

[25] R. Xiong, H. Y. Meng, Q. Q. Yao, B. Huang, Y. M. Liu, H. C. Xue, *et al.*, "Simultaneous measurement of refractive index and temperature based on modal interference," *IEEE Sensors Journal*, 2014, 14(8): 2524–2528.

[26] L. Q. Wang, L. Yang, C. Zhang, C. Y. Miao, J. F. Zhao, and W. Xu, "High sensitivity and low loss open-cavity Mach-Zehnder interferometer based on multimode interference coupling for refractive index measurement," *Optics and Laser Technology*, 2019, 109: 193–198.